JCI insight

TECHNICAL ADVANCE

Targeting the human MUC1-C oncoprotein with an antibody-drug conjugate

Govind Panchamoorthy,[1] Caining Jin,[2] Deepak Raina,[1] Ajit Bharti,[3] Masaaki Yamamoto,[2] Dennis Adeebge,[4] Qing Zhao,[3] Roderick Bronson,[5] Shirley Jiang,[2] Linjing Li,[2] Yozo Suzuki,[2] Ashujit Tagde,[2] P. Peter Ghoroghchian,[2] Kwok-Kin Wong,[4] Surender Kharbanda,[1,2] and Donald Kufe[2]

[1]Genus Oncology, Boston, Massachusetts, USA. [2]Dana-Farber Cancer Institute, Harvard Medical School, Boston, Massachusetts, USA. [3]Departments of Medicine and Pathology, Boston University School of Medicine, Boston, Massachusetts, USA. [4]Laura and Isaac Perlmutter Cancer Center, New York University Langone Medical Center, New York, New York, USA. [5]Division of Immunology, Department of Microbiology and Immunobiology, Harvard Medical School, Boston, Massachusetts, USA.

Mucin 1 (MUC1) is a heterodimeric protein that is aberrantly overexpressed on the surface of diverse human carcinomas and is an attractive target for the development of mAb-based therapeutics. However, attempts at targeting the shed MUC1 N-terminal subunit have been unsuccessful. We report here the generation of mAb 3D1 against the nonshed oncogenic MUC1 C-terminal (MUC1-C) subunit. We show that mAb 3D1 binds with low nM affinity to the MUC1-C extracellular domain at the restricted α3 helix. mAb 3D1 reactivity is selective for MUC1-C–expressing human cancer cell lines and primary cancer cells. Internalization of mAb 3D1 into cancer cells further supported the conjugation of mAb 3D1 to monomethyl auristatin E (MMAE). The mAb 3D1-MMAE antibody-drug conjugate (ADC) (a) kills MUC1-C–positive cells in vitro, (b) is nontoxic in MUC1-transgenic (MUC1.Tg) mice, and (c) is active against human HCC827 lung tumor xenografts. Humanized mAb (humAb) 3D1 conjugated to MMAE also exhibited antitumor activity in (a) MUC1.Tg mice harboring syngeneic MC-38/MUC1 tumors, (b) nude mice bearing human ZR-75-1 breast tumors, and (c) NCG mice engrafted with a patient-derived triple-negative breast cancer. These findings and the absence of associated toxicities support clinical development of humAb 3D1-MMAE ADCs as a therapeutic for the many cancers with MUC1-C overexpression.

Introduction

Mucin 1 (MUC1) is a heterodimeric protein that is aberrantly overexpressed by diverse types of carcinomas, including those of the breast and lung (1, 2). Based on these and other findings, the National Cancer Institute Project for the Acceleration of Translational Research ranked MUC1 as the second-most promising cancer antigen among 75 candidates (3). MUC1 is translated as a single polypeptide, which undergoes autocleavage into two subunits at a sea urchin sperm protein, enterokinase, agrin (SEA) domain (1, 2). The MUC1 N-terminal (MUC1-N) subunit contains highly glycosylated tandem repeats that are a physical characteristic of the mucin family (1, 2). MUC1-N forms a complex with the MUC1 C-terminal (MUC1-C) subunit at the cell membrane and is shed from the surface of cancer cells in association with increased plasma levels (1, 2). In this context, the clinical development of mAbs, such as AS1402 (huHMFG-1) and BrevaRex (AR-20.5), directed against the MUC1-N subunit was unsuccessful, in part because of the circulating pools of MUC1-N that preclude targeting of antibodies to the surface of tumor cells (4–7). By contrast, the nonshed MUC1-C subunit, which functions as an oncoprotein, represents an attractive target for the development of mAb-based therapeutics (1, 2, 8).

MUC1-C consists of a 58-aa extracellular domain, a 28-aa transmembrane domain, and a 72-aa cytoplasmic tail (1, 2). The MUC1-C extracellular domain (MUC1-C/ED) has a single motif for N-glycosylation, which, in turn, functions as a binding site for galectin-3 (9) and includes α3 and α4 helices, as determined by NMR spectroscopy (10). The MUC1-C cytoplasmic tail is an intrinsically disordered protein, as is found in oncoproteins that intersect with multiple signaling pathways (11). The MUC1-C cytoplasmic domain is thus phosphorylated by diverse kinases and directly interacts with effectors of signaling pathways that have been linked to oncogenesis (1, 2, 8). In this way, MUC1-C contributes to loss

Authorship note: GP and CJ contributed equally to this work.

Conflict of interest: DK has equity interests in, serves as a member of the board of directors of, and is a paid consultant for Genus Oncology.

Submitted: January 17, 2018
Accepted: May 3, 2018
Published: June 21, 2018

Reference information:
JCI Insight. 2018;3(12): e99880.
https://doi.org/10.1172/jci.insight.99880.

of polarity, the cancer stem cell state, epithelial-mesenchymal transition, and epigenetic programming of cancer cells (8, 12). Moreover, MUC1-C integrates the epithelial-mesenchymal transition program with induction of the programmed death ligand 1 (PD-L1) and immune evasion (12–15). In concert with these findings, overexpression of MUC1-C in breast and lung carcinomas is associated with induction of gene signatures that are predictive of significant decreases in disease-free and overall survival, further supporting the attractiveness of MUC1-C as a cancer target (16–18).

The present studies describe the development of what to our knowledge is a first-in-class mAb, designated 3D1, which reacts specifically with the MUC1-C/ED at the α3 helix. We show that mAb 3D1 binds selectively and with high affinity to the surface of MUC1-C–expressing human cancer cells. The results demonstrate that mAb 3D1 and the humanized mAb (humAb) 3D1 are highly effective as antibody-drug conjugates (ADCs) in delivery of the payload, monomethyl auristatin E (MMAE), to cancer cells growing in vitro and as tumors in mouse models.

Results

Interaction of mAb 3D1 with the α3 helix in the MUC1-C/ED. MUC1 was translated as a single polypeptide that undergoes autocleavage within a conserved G^SVVV motif in the extracellular SEA domain (10, 19, 20) (Supplemental Figure 1A; supplemental material available online with this article; https://doi.org/10.1172/jci.insight.99880DS1). In turn, the resulting MUC1-N and MUC1-C terminal subunits formed a stable heterodimer that was expressed at the cell membrane (Supplemental Figure 1B, top). The generation of mAbs against the MUC1-C/ED has been limited, at least in part, by a lack of understanding how the heterodimer forms. For this reason, we identified a putative structure for the extracellular MUC1-N/MUC1-C heterodimer, which aligns the MUC1-N LGL motif with the MUC1-C LTL motif (Supplemental Figure 1B, bottom). In support of this structure, incubation of a MUC1-N 62-aa fragment (p62; Supplemental Figure 1C, left) with the MUC1-C 58-aa extracellular domain (MUC1-C/ED; Supplemental Figure 1C, right) resulted in the formation of a heterodimer (Supplemental Figure 1D, left). The importance of the LXL motifs in stabilizing this extracellular heterodimer was further supported by the demonstration that the interaction was abrogated by the p62 LGL→AGA and MUC1-C/ED LTL→ATA mutations (Supplemental Figure 1D, right).

Hybridomas generated from the immunized mice were screened for reactivity against the MUC1-N p62/MUC1-C/ED p58 heterodimer. Clone 3D1 was selected from this screen based on reactivity with a K_D of 17 nM, as determined by surface plasmon resonance (Figure 1A). As a control, an IgG1 isotype identical mAb, CD1, which reacts with the MUC1-C cytoplasmic domain (21), had no detectable binding (Figure 1B). Disruption of the MUC1-N p62/MUC1-C/ED p58 heterodimer formation with L→A mutations had no apparent effect on mAb 3D1 binding (Figure 1B), indicating that the 3D1 antibody is not reactive with the MUC1-N/MUC1-C junction. In addition, mAb 3D1 had no detectable binding to MUC1-N p62 (Figure 1B), suggesting that the epitope resides in the MUC1-C/ED p58 region. MUC1-C/ED includes a predicted α3 helix (α3: VHDVETQFNQ) (10) that is largely conserved in humans, cynomolgus monkeys, and mice (Figure 1C). Using site-directed mutagenesis to determine if the α3 helix is the mAb 3D1 epitope, we found that reactivity of mAb 3D1 was decreased in part by mutation of the MUC1-C/ED D19 residue to glutamic acid (D19E) (Figure 1D). Moreover, mutation of the other conserved V20 and T22 residues abrogated mAb 3D1 binding (Figure 1D), clearly demonstrating that mAb 3D1 binds to the α3 helix (Figure 1E).

Selectivity of mAb 3D1 for MUC1-C–expressing carcinoma cells. A BLAST search demonstrated that the α3 helix sequence is restricted to MUC1-C, indicating that mAb 3D1 reactivity should be selective for MUC1-C–expressing cancer cells. To assess selectivity of mAb 3D1 binding, we first performed studies with MUC1-null HCT116 colon cancer cells, which were transfected to stably express an empty vector or MUC1 (22). In this model, mAb 3D1 reactivity was detectable with HCT116/MUC1 as compared with HCT116/vector cells (Figure 2A). These results were confirmed in studies demonstrating that mAb 3D1 selectively binds to HCT116/MUC1 cells with a half-maximal concentration (EC_{50}) of 16.4 nM (Figure 2B). We also studied MDA-MB-468 triple-negative breast cancer (TNBC) cells expressing a control shRNA (CshRNA) or a MUC1-targeting shRNA in order to knock down MUC1-C expression (23). We found that binding of mAb 3D1 to MDA-MB-468/MUC1 shRNA cells was substantially decreased compared with that in MDA-MB-468/CshRNA cells (Figure 2C), providing further support for selectivity of this antibody against MUC1-C–expressing cells. In concert with the findings from these MUC1 knockin and knockdown studies, analysis of (a) the HCC827 and H441 non–small cell lung cancer (NSCLC) lines, which constitutively

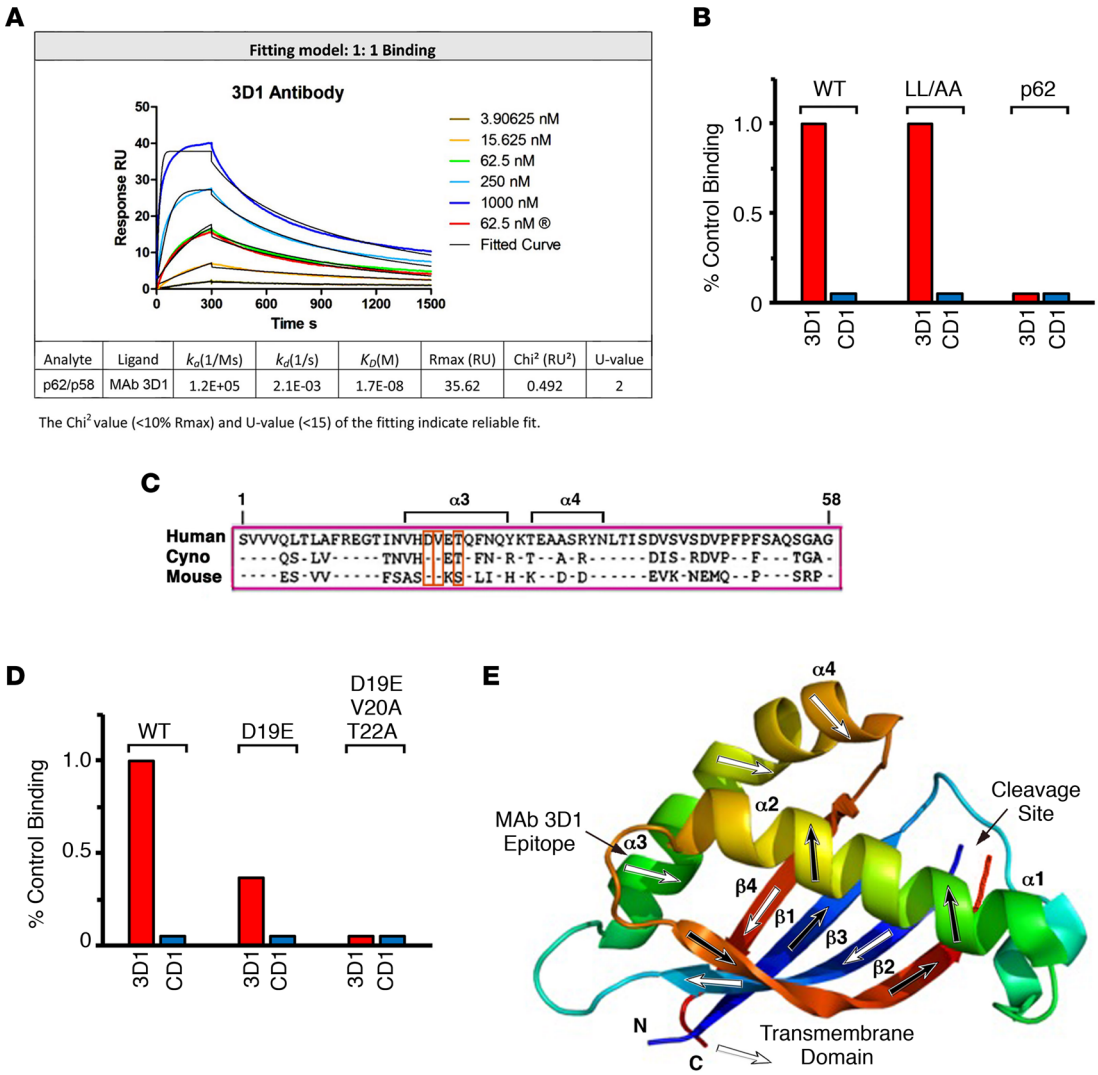

Figure 1. mAb 3D1 binds to MUC1-C/ED at the α3 helix. (**A**) mAb 3D1 binding to the MUC1 p62/p58 heterodimer was determined by surface plasmon resonance (SPR). Listed below are the indicated parameters of the binding analysis. (**B**) Binding of mAb 3D1 by ELISA to the (a) WT MUC1 p62/p58 heterodimer, (b) p62 (LGL→AGA) and p58 (LTL→ATA) mutant proteins that do not form the p62/p58 junction, and (c) WT p62 alone. mAb CD1, which reacts with the MUC1-C cytoplasmic domain, was used as a control. The results are expressed as percentage of control binding as compared with that obtained with the WT protein (>3.0 OD units). (**C**) The aa sequences of the 58-aa human MUC1-C, cynomolgus monkey, and mouse Muc1-C extracellular domains. The α3 and α4 helices are highlighted. (**D**) Binding of mAb 3D1 by ELISA to WT p58 and the D19E or D19E/V20A/T22A mutant proteins. mAb CD1 was used as a control. The results are expressed as percentage control binding as compared with that obtained with the WT protein (>3.0 OD units). (**E**) Localization of the mAb 3D1 epitope to the α3 helix, as shown by NMR spectroscopy of the p62/p58 heterodimer (adapted from Macao et al., ref. 10).

express MUC1-C (24, 25), and (b) primary NSCLC cells from a resected tumor demonstrated mAb 3D1 reactivity with over 95% of these cells (Figure 2, D and E, and Supplemental Figure 2). Similar results were obtained with ZR-75-1 luminal breast cancer cells (Figure 2F), indicating that mAb 3D1 binds to the surface of diverse types of carcinoma cells.

To extend these lines of investigation, we next studied mAb 3D1 reactivity in formalin-fixed, paraffin-embedded (FFPE) sections of representative MUC1-expressing tumors. As determined by IHC, mAb 3D1 staining was detectable throughout a ductal breast carcinoma (Figure 3A, left) and was selective for cancer cells, as compared with normal ductal epithelial cells (Figure 3A, right). Selectivity of mAb 3D1 reactivity for carcinoma cells was also found from staining of a (a) NSCLC of the adenocarcinoma subtype (Figure 3B) and (b) gastric carcinoma (Figure 3C).

mAb 3D1 is effective in delivering MMAE to MUC1-C–positive cancer cells in vitro and in vivo. mAb 3D1 was labeled with Alexa Fluor 488 to assess whether binding to the surface of carcinoma cells is associated with internalization. As a representative experiment, incubation of HCT116/MUC1-C cells

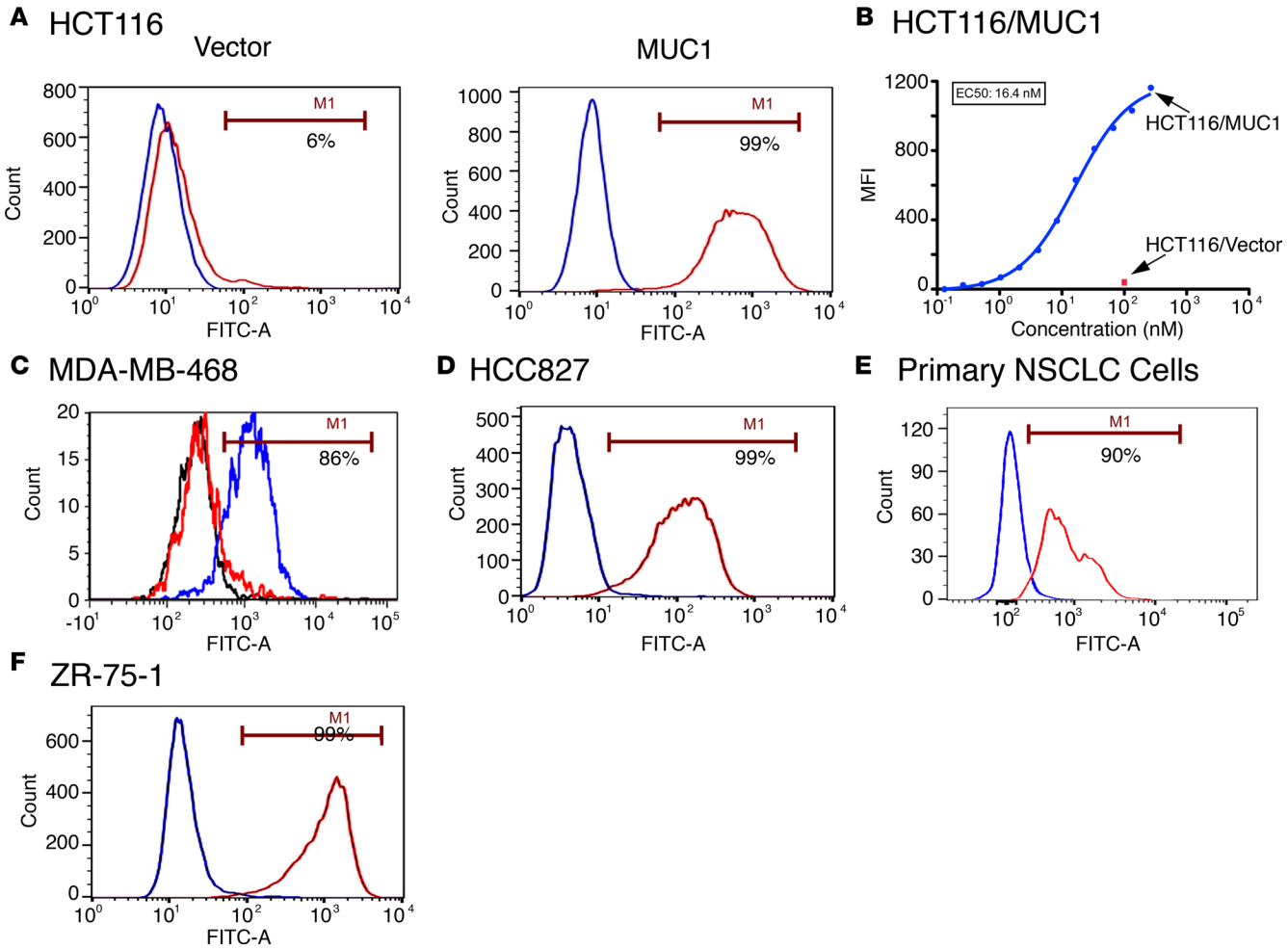

Figure 2. mAb 3D1 binds selectively to MUC1-C–expressing cancer cells. (**A**) HCT116/vector and HCT116/MUC1 cells were incubated with mAb 3D1 (red) or control mAb CD1 (blue) and analyzed by flow cytometry. The percentage of mAb 3D1 positive cells is noted. (**B**) The indicated concentrations of mAb 3D1 were incubated with HCT116/vector or HCT116/MUC1 cells. Mean fluorescence intensity (MFI) was determined by flow cytometry. (**C**) MDA-MB-468 cells expressing a control CshRNA (blue) or a MUC1 shRNA (red) were analyzed for mAb 3D1 binding by flow cytometry. mAb CD1 reactivity with MDA-MB-468/CshRNA cells (black) is included as a control. (**D**–**F**) HCC827 NSCLC cells (**D**), primary NSCLC cells from a resected tumor (**E**), and ZR-75-1 breast cancer cells (**F**) were incubated with mAb 3D1 (red) or control mAb CD1 (blue) and analyzed by flow cytometry.

with mAb 3D1–Alexa Fluor 488 was associated with cell surface binding at 4°C and internalization at 37°C (Figure 4A). By contrast, there was no detectable internalization of mAb 3D1–Alexa Fluor 488 in studies with HCT116/vector cells (Supplemental Figure 3). Based on these findings, we conjugated mAb 3D1 to MMAE using the cleavable maleimido caproyl-valine-citrulline linker. Incubation of mAb 3D1-MMAE with HCT116/vector and HCT116/MUC1 cells demonstrated MUC1-C–dependent killing with a half-maximal lethal concentration (LC_{50}) of 3.8 nM (Figure 4B). In concert with these results, mAb 3D1-MMAE was effective in killing MDA-MB-468/CshRNA, but not MDA-MB-468/MUC1 shRNA, cells (Figure 4C) and HCC827 cells (Figure 4D) at low nM concentrations.

To assess potential delivery of the ADC in vivo, pharmacokinetic studies of mAb 3D1 were first performed by administering doses of 5 and 10 mg/kg i.v. in C57BL/6 mice. The C_{max} and area under the curve (AUC_{0-t}) were proportional to the administered dose (Supplemental Table 1). Additionally, the elimination half-life ($t_{1/2}$ = ~9 days) was similar for both doses (Supplemental Figure 4 and Supplemental Table 1), indicating favorable pharmacokinetics in mice. Based on these findings, mAb 3D1-MMAE ADCs were administered as a single dose of 15 mg/kg i.v. to human MUC1-transgenic (MUC1.Tg) mice, which express MUC1 in a pattern and at levels found in humans (26). Notably, there was no evidence of (a) weight loss and other overt toxicities or (b) histopathologic damage to the multiple MUC1-expressing normal tissues, including the lung, colon, and kidney (Supplemental Figure 5). mAb 3D1-MMAE ADCs were then administered to nude

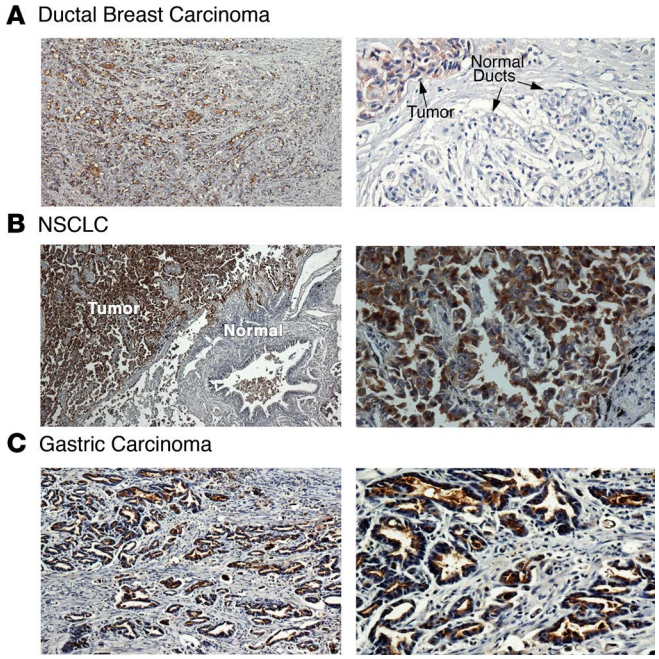

Figure 3. mAb 3D1 reactivity is selective for human carcinomas. (**A**–**C**) Formalin-fixed, paraffin-embedded (FFPE) sections of a ductal breast carcinoma (**A**), NSCLC of the adenocarcinoma subtype (**B**), and a gastric carcinoma (**C**) were immunostained with mAb 3D1 using an indirect IHC assay. Original magnification, ×4 (left column); ×10 (**A**, right column); ×20 (**B** and **C**, right column).

mice with established HCC827 tumor xenografts. Treatment with mAb 3D1-MMAE at a dose of 5 mg/kg i.v. each week for 3 weeks was associated with a marked inhibition of tumor growth (Figure 4E). In addition, there was no evidence of weight loss (Supplemental Figure 6) or other overt toxicities in this model.

Humanization of mAb 3D1. Based on the above findings, mAb 3D1 was humanized by complementarity determining region (CDR) grafting. HumAb 3D1 clones analyzed by BIAcore and FACS titration were ranked by affinity for selection of the candidate humAb 3D1. As found for mouse mAb 3D1, reactivity of humAb 3D1 was selective for HCT116 cells expressing MUC1 at an EC_{50} of 13 nM (Supplemental Figure 7). To assess the distribution of humAb 3D1 in vivo, we generated mouse MC-38 colon cancer cells that stably express an empty (MC-38/vector) or MUC1 (MC-38/MUC1) vector. Reactivity of humAb 3D1 was detectable on the surface of MC-38/MUC1, and not MC-38/vector, cells (Supplemental Figure 8A). MUC1.Tg mice are tolerant to MUC1 and thereby represent an immunocompetent model for the growth of MC-38/MUC1 tumors (27). We therefore used this model to assess the effects of humAb 3D1 conjugated to MMAE. Administration of humAb 3D1-MMAE ADCs at a single dose of 10 mg/kg i.v. resulted in significant inhibition of MC-38/MUC1 tumor growth (Supplemental Figure 8B). In concert with the above studies with mAb 3D1-MMAE ADCs in MUC1.Tg mice, i.v. administration of humAb 3D1-MMAE ADCs had no effect on body weight (Supplemental Figure 8C) and no adverse effects on MUC1-C–expressing normal tissues. We also found that i.v. dosing of humAb 3D1-MMAE ADCs at 10 mg/kg once or 5 mg/kg/wk for 3 weeks had no effect on blood chemistry values (Supplemental Table 2) or hematologic parameters (Supplemental Table 3).

Activity of humAb 3D1-MMAE ADCs against human cancer cells. As demonstrated for mAb 3D1-MMAE ADCs, the humAb 3D1-MMAE ADCs were effective in killing HCT116/MUC1, but not HCT116/vector, cells (Figure 5A; LC_{50} = 13 nM), and HCC827 cells (Figure 5B; LC_{50} = 9 nM). In addition, the effects of treating ZR-75-1 cells with humAb 3D1-MMAE ADCs (LC_{50} = 1.2 nM) were comparable to those obtained with mAb 3D1-MMAE ADCs (LC_{50} = 1.3 nM) (Figure 5C), in concert with the similar affinities of the mouse and humanized 3D1 antibodies. To further assess antitumor activity of the humAb 3D1-MMAE ADCs, nude mice with established ZR-75-1 tumor xenografts (~200 mm^3) were treated i.v. with 5 mg/kg/wk for 3 weeks. In this model, administration of the humAb 3D1-MMAE ADCs was associated with tumor regressions and durable responses (Figure 5D). MUC1-C is overexpressed in approximately 90% of TNBCs and is an attractive target for the treatment of this aggressive disease (28). Accordingly, NCG mice harboring a patient-derived xenograft (PDX) TNBC tumor, which expresses MUC1-C, were treated i.v. with humAb 3D1-MMAE ADCs at 5 mg/kg/wk for 3. As found in the ZR-75-1 xenograft model, treatment of the PDX TNBC tumors resulted in durable responses (Figure 5E).

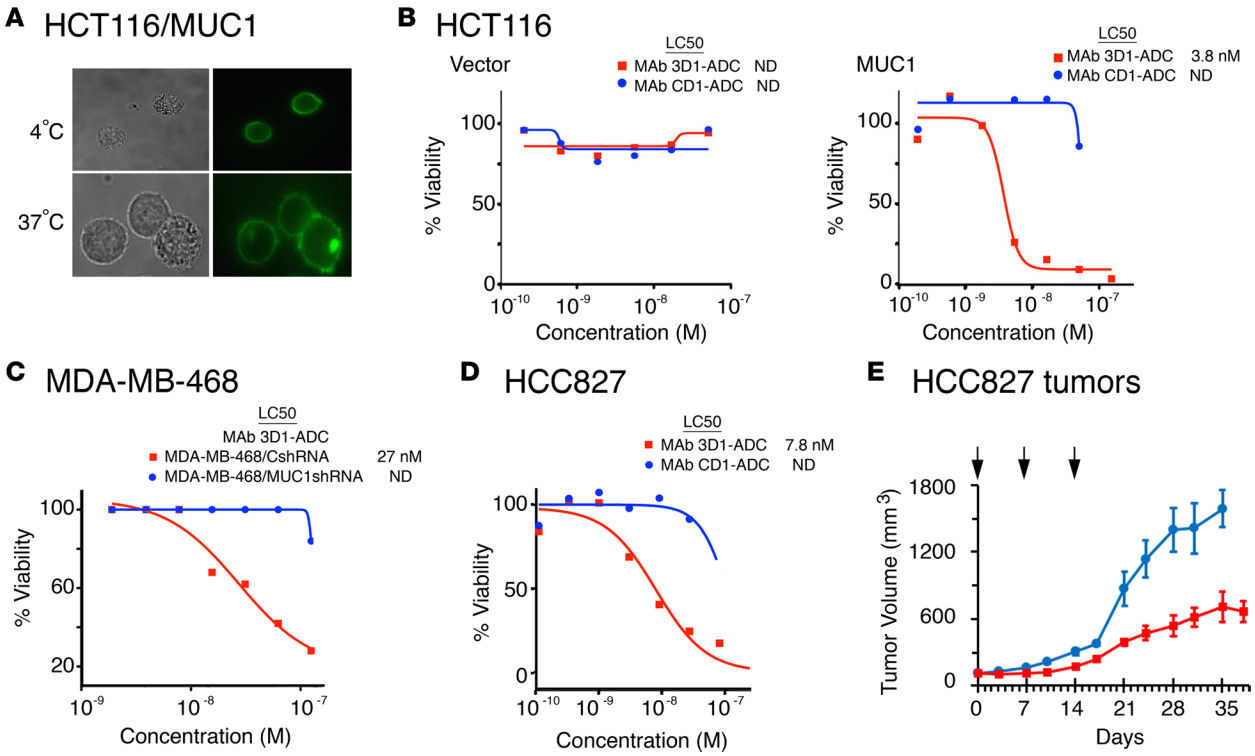

Figure 4. Activity of mAb 3D1-MMAE ADCs against MUC1-C–expressing cancer cells. (**A**) mAb 3D1 labeled with Alexa Fluor 488 was incubated with HCT116/MUC1 cells for 3 hours at the indicated temperatures. Cells were visualized by phase-contrast (left) and fluorescence (right) microscopy. Original magnification, ×60. (**B**) HCT116/vector and HCT116/MUC1 cells were incubated with the indicated concentrations of mAb 3D1-MMAE ADCs (red squares) or mAb CD1-MMAE ADCs (blue circles). Percentage viability was determined by Alamar blue staining. The LC_{50} values are noted. ND, not determined. (**C**) MDA-MB-468/CshRNA (red squares) and MDA-MB-468/MUC1 shRNA (blue circles) were incubated with the indicated concentrations of mAb 3D1-MMAE ADCs. Percentage viability was determined by Alamar blue staining. (**D**) HCC827 cells were incubated with the indicated concentrations of mAb 3D1-MMAE ADCs (red squares) or mAb CD1-MMAE ADCs (blue circles). Percentage viability was determined by Alamar blue. (**E**) Nude mice bearing HCC827 tumor xenografts (~150 mm^3) were pair matched and then treated with vehicle control (blue circles) or mAb 3D1-MMAE ADCs at a dose of 5 mg/kg/wk for 3 weeks (red squares). The results are expressed as tumor volumes (mean ± SEM; 6 mice per group).

Discussion

The MUC1-C oncoprotein is a highly attractive target based on its aberrant overexpression in many types of carcinomas (Supplemental Figure 9). The importance of MUC1-C in driving the epithelial-mesenchymal transition program, the cancer stem cell state, drug resistance, and immune evasion has further emphasized a critical need for developing agents against this target (8, 12–15). The present results describe the development of an antibody, designated 3D1, which reacts with high affinity to the MUC1-C/ED. mAb 3D1 reacts specifically with MUC1-C on the cancer cell surface, as evidenced by flow cytometry studies comparing isogenic cells with knockin and knockdown of MUC1 expression. We also found that mAb 3D1 binds to the surface of multiple NSCLC and breast cancer cell lines. By extension, mAb 3D1 reactivity was similarly detected on the surface of primary NSCLC cells from a resected tumor. Staining of sections from FFPE tumors further showed mAb 3D1 reactivity with breast, NSCLC, and gastric cancer cells but not surrounding normal epithelia, supporting a breadth of carcinomas that could be selectively targeted with this antibody.

Epitope mapping showed that mAb 3D1 binds to the MUC1-C/ED α3 helix, which is also present in Muc1-C proteins from cynomolgus monkeys and mice. In this regard, mAb 3D1 binds with similar affinity to MUC1-C/ED derived from humans, cynomolgus monkeys, and mice. Junctional mAbs generated against the SEA region encompassing the shed MUC1-N and MUC1-C subunits have been limited by extent of internalization and absence of antitumor activity (29, 30). By contrast, the specific targeting of the MUC1-C/ED α3 helix has not been previously described to our knowledge. Another characteristic of relevance for the development of mAb 3D1 is that binding of this antibody to the cancer cell surface is associated with internalization, indicating that mAb 3D1 could be employed for the delivery of payloads. Indeed, we found that conjugating mAb 3D1 to MMAE is highly effective as an ADC for killing MUC1-C–expressing cancer cells at low nM concentrations. We also found that mAb-3D1-MMAE treatment is effective in inhibiting growth of established HCC827

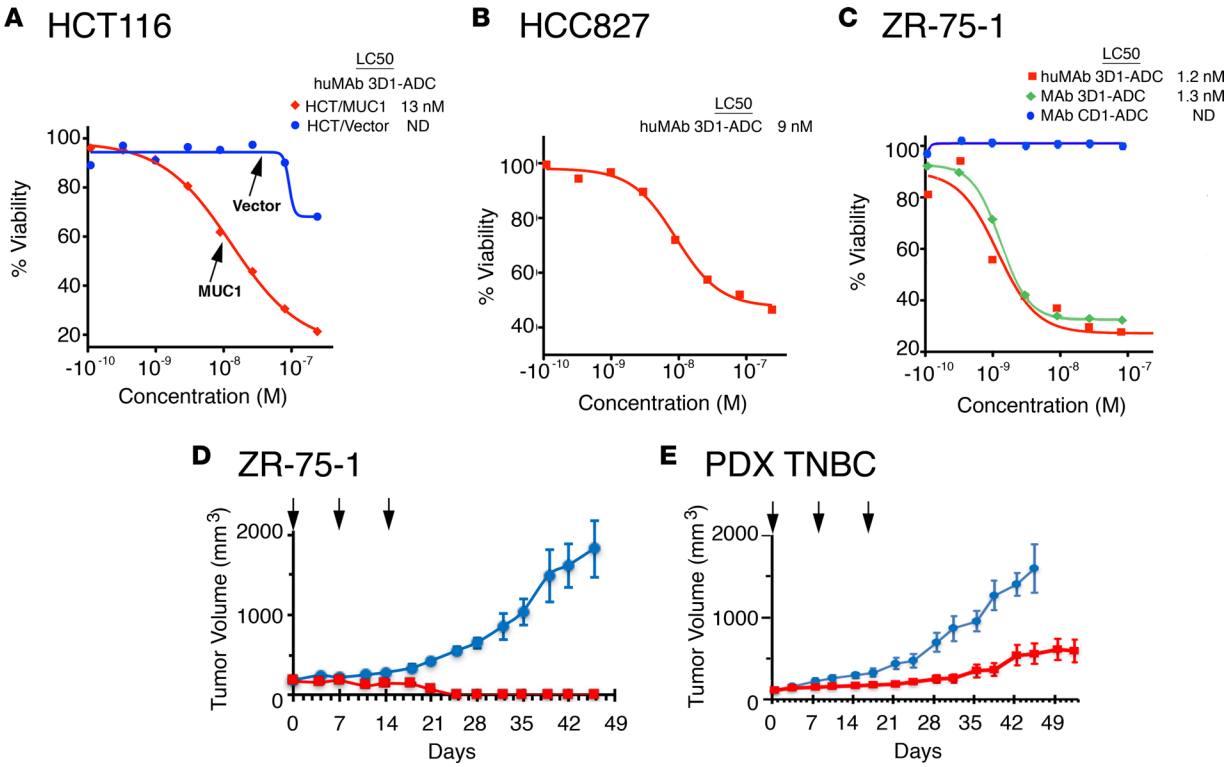

Figure 5. HumAb 3D1-MMAE ADCs are active against human tumor models. (**A** and **B**) HCT116/vector (**A**; blue circles), HCT116/MUC1 (**A**; red diamonds), and HCC827 (**B**) cells were incubated with the indicated concentrations of humAb 3D1-MMAE ADCs. (**C**) ZR-75-1 cells were incubated with the indicated concentrations of humAb 3D1-MMAE ADCs (red squares), mAb 3D1-MMAE ADCs (green diamonds), or mAb CD1-MMAE ADCs (blue circles). Percentage viability was determined by Alamar blue. (**D**) Nude mice bearing ZR-75-1 tumor xenografts (~200 mm^3) were pair matched and then treated i.v. with vehicle control (blue circles) or humAb 3D1-MMAE ADCs at a dose of 5 mg/kg/wk for 3 weeks (red squares). The results are expressed as tumor volumes (mean ± SEM; 6 mice per group). (**E**) NCG mice bearing PDX TNBC tumor xenografts (~150 mm^3) were pair matched and then treated i.v. with vehicle control (blue circles) or humAb 3D1-MMAE ADCs at a dose of 5 mg/kg/wk for 3 weeks (red squares). The results are expressed as tumor volumes (mean ± SEM; 6 mice per group).

NSCLC xenografts in nude mice in the absence of weight loss or other apparent toxicity. This lack of toxicity was of interest in that (a) mouse Muc1-C is expressed on normal epithelial tissues and (b) mAb 3D1 recognizes mouse Muc1-C/ED with a similar affinity to that obtained for human MUC1-C/ED. These findings indicated that the mAb-3D1-MMAE ADC selectively targets MUC1-C on tumor cells and not Muc1-C on normal tissues.

MUC1.Tg mice represent an excellent model for further assessing the toxicity of mAb 3D1-MMAE ADCs in a setting in which human MUC1-C is expressed in normal epithelial tissues in a pattern and at a level comparable to that found in humans (26). In addition, tolerance of MUC1.Tg mice to human MUC1-C provides an opportunity for assessing the activity of these ADCs against MUC1-C–expressing syngeneic tumor cells. Based on these aspects of the model, the mAb 3D1-MMAE ADCs were administered to MUC1.Tg mice bearing MC-38/MUC1-C tumors. We found that the ADCs induced antitumor activity in the absence of toxicity to MUC1-C–expressing normal tissues. One explanation for this selectivity is that MUC1-C is overexpressed in cancer cells as compared with that in normal epithelia. Additionally, MUC1-C expression is restricted to the apical borders of normal epithelial cells (26). By contrast, carcinoma cells exhibit loss of apical-basal polarity and MUC1-C is expressed over the entire cell surface (1), invoking the notion that tumors may be more readily accessible to antibodies, and potentially other immune effectors, than the apical borders of epithelial cells facing the external environment. Thus, mAb 3D1–mediated approaches against MUC1-expressing tumors could have highly favorable therapeutic profiles because of distinct levels and patterns of MUC1-C expression on cancer cells as compared with normal cells.

The development of mAb-3D1 ADCs to target the diverse types of carcinomas that overexpress the MUC1-C oncoprotein offers numerous opportunities for cancer treatment (1, 2). The available evidence indicates that MUC1-C integrates epithelial-mesenchymal transition and the cancer stem cell state with epigenetic reprogramming and drug resistance of carcinoma cells (8), further establishing MUC1-C as a highly important target for refractory tumor cell populations. Accordingly, mAb 3D1 was humanized for

clinical development, noting that humAb 3D1 retains the binding affinity and specificity for MUC1-C/ED, as demonstrated for the mouse antibody. In addition, the humAb-3D1-MMAE ADCs are active against carcinoma cells in vitro and in in vivo models. Based on these findings, the humAb-3D1-MMAE ADC is being advanced to investigational new drug–enabling studies as a strategy for the immunotherapy of cancer. Of further interest in this regard is the previously unrecognized role for MUC1-C in promoting immune evasion by driving PD-L1 expression and suppressing that of immune effectors, such as IFN-γ, in NSCLC cells (14). As a result, targeting MUC1-C function with the GO-203 inhibitor of the intracellular domain downregulates PD-L1, induces IFN-γ, and enhances effector activity of $CD8^+$ tumor-infiltrating T cells in MUC1.Tg mouse models of NSCLC and TNBC (15, 31) and in patients with acute myelogenous leukemia (32). These findings have highlighted the potential for targeting MUC1-C–expressing cancer cells as an approach for reprogramming of the tumor microenvironment.

In summary, humAb-3D1-MMAE ADC-mediated killing of cancer cells could be effective in reversing the suppressive immune microenvironment of tumors, thereby enhancing the activity of other immunotherapeutic agents, including antibodies used for blockade of the PD-1/PD-L1 axis. mAb 3D1 could also be useful in targeting MUC1-C–expressing cancers with other approaches, including antibody-dependent cell-mediated cytotoxicity, T cell–engaging bispecific formats, and the design of CAR-T cells.

Methods

Generation of anti-MUC1-C/ED antibody. Swiss-Webster mice (The Jackson Laboratory) were injected subcutaneously and i.p. with 100 μg MUC1-C/ED protein in PBS emulsified with Complete Freund's adjuvant and CpG adjuvant. The mice were boosted i.p. at 2-week intervals after the initial immunization with MUC1-C/ED protein in Freund's incomplete adjuvant and CpG adjuvant. A final boost was performed i.v. with MUC1-C/ED protein in PBS. Immune sera from the immunized mice were screened by (a) flow cytometry of MUC1-positive and MUC1-negative cell lines and (b) reactivity with MUC1-C/ED protein using an ELISA. Four days after the final boost, spleens from selected mice were harvested for fusion with mouse sp2/0-Ag14 myeloma cells. The mAb 3D1 hybridoma selected by screening supernatants with flow cytometry and ELISA was subjected to subcloning by limiting dilution to obtain a clonal cell population.

Cell culture. Human HCT116 colon cancer cells (ATCC) transduced to stably express an empty vector or MUC1 (22), human MDA-MB-468 breast cancer cells (ATCC) transduced to express a control scrambled CshRNA or a MUC1 shRNA (23), and mouse MC-38 colon cancer cells (provided by J. Schlom, National Cancer Institute, Bethesda, Maryland, USA) transduced to stably express an empty vector or MUC1 were cultured in Dulbecco's modified Eagle's medium supplemented with 10% heat-inactivated fetal bovine serum (HI-FBS), 100 μg/ml streptomycin, and 100 units/ml penicillin. Human HCC827 NSCLC, H441 NSCLC, and ZR-75-1 breast cancer cells (ATCC) were grown in RPMI1640 medium supplemented with HI-FBS, streptomycin, and penicillin. Cell growth was assessed by trypan blue staining. Authentication of the cells was performed by short tandem repeat analysis. Cells were monitored for mycoplasma contamination by a MycoAlert Mycoplasma Detection Kit (Lonza).

Primary NSCLC cells. Resected NSCLC tumor was processed for analysis by flow cytometry as described previously (33).

Flow cytometry. Cells were blocked by incubation with 1% BSA/PBS for 20 minutes on ice. After washing, the cells were incubated with 4 g/ml mAb 3D1 or an IgG1 isotype control antibody for 60 minutes on ice. FITC-conjugated goat F(ab′)2 anti-mouse immunoglobulin was used as the secondary reagent (catalog 115-096-146, Jackson ImmunoResearch). Antibody binding to the cell surface was analyzed using FACS Canto II and FACSDiva software (BD Biosciences).

ELISA. ELISA plate wells were coated overnight with 100 μl of a 1 μg/ml solution of the target proteins. Varying concentrations of mAb 3D1 or a control antibody were incubated with the coated proteins for 1 hour at room temperature. Bound primary antibody was detected by incubation with HRP-conjugated goat anti-mouse IgG (1:500 dilution; catalog 115-035-072, GE Healthcare Life Sciences). After development for 30 minutes in the presence of ABTS (Kirkegaard and Perry Laboratories), the wells were read at 405 nm using a ThermoMax plate reader (Molecular Devices) and SoftMax Pro (Molecular Devices).

Surface plasmon resonance. mAb 3D1 was immobilized in the second flow cell of Series S sensor chip CM5 (GE Healthcare) using the amine-coupling method followed by blocking with ethanolamine. MUC1-C/ED was passed through the chip at 30 μl/min for an association time of 300 seconds and a disassociation time

of 1,200 seconds. Data obtained from the sensograms were analyzed using the BIAcore T200 evaluation software, Langmuir binding model (GE Healthcare), and GraphPad Prism (GraphPad Software).

Assessment of antibody internalization. mAb 3D1 and a control CD1 antibody reactive with the MUC1-C cytoplasmic domain (21) were labeled using the Alexa Fluor 488 Monoclonal Antibody Labeling Kit (catalog A20181; Invitrogen). The Alexa Fluor 488–labeled antibodies were incubated with cells on ice for 60 minutes. The cells were then washed with PBS, incubated for an additional 3 hours at 37°C, and monitored for internalization using the Nikon deconvolution wide-field epifluorescence system. Images were captured using NIS-Element software and analyzed by ImageJ (NIH) software.

IHC analysis. An indirect IHC assay for immunostaining FFPE tissues with mAb 3D1 was developed using the Intellipath auto-stainer (Biocare Medical) as described previously (34).

Generation of ADCs. mAb 3D1, humAb 3D1, and the CD1 control antibody (21) were conjugated to MMAE (Moradec) with a cleavable linker as described previously (35, 36). The drug-to-antibody ratio was determined by the A_{248nm}/A_{280nm} method (37) and ranged from 2.8 to 4.2. ADC-mediated cell killing was determined by the Alamar blue conversion assay (Invitrogen).

Pharmacokinetic studies. mAb 3D1 (100 μl) was administered at doses of 5 and 10 mg/kg to C57BL/6 mice (12–16 weeks old; mean body weight, 21 grams; The Jackson Laboratory) by retro-orbital injection. Blood samples were collected in BD Microtainer tubes (Becton Dickinson) from the mandibular vein. Serum mAb 3D1 concentrations were determined by ELISA.

Mouse tumor models. Six- to eight-week-old nude mice (Taconic Farms) were injected subcutaneously in the flank with 5×10^6 HCC827 or ZR-75-1 tumor cells in 100 μl of a 1:1 solution of medium and Matrigel (BD Biosciences). In the MUC1.Tg mouse model, 5×10^5 MC-38/MUC1 cells were injected subcutaneously in the flank. For the PDX model, patient-derived triple-negative breast tumor fragments (DFBC11-26; ~2 × 2 mm) were implanted into each of the third mammary fat pads of 6- to 8-week-old NCG mice (Charles River Laboratories) (38). Mice were randomized into treatment groups when the mean tumor volume reached 100–200 mm^3. Tumor measurements and body weights were recorded twice a week. Mice were sacrificed when tumors reached >1,000 mm^3 as calculated by the following formula: $(\text{width})^2 \times \text{length}/2$.

Humanization of mAb 3D1. Humanization of mouse mAb 3D1 was performed by CDR grafting. Sequences from the CDR regions of the heavy and light chains were used to search for homologous sequences from the human germline database using NCBI Ig-Blast. Corresponding sequences were synthesized and integrated into a human IgG1 containing pTGE5 vector. Affinity ranking of chimeric and humanized antibodies was performed using FACS titration and SPR with BIACore T200 (GE Healthcare).

Statistics. Each experiment was repeated at least 3 times. Data are expressed as mean ± SD. The paired 1-tailed Student's *t* test was used to examine differences between means of two groups. A *P* value of less than 0.05 was considered a statistically significant difference.

Study approval. Animal studies were performed under animal protocols (03-029 and 12-029) approved by the Dana-Farber Cancer Institute Animal Use and Care Committee.

Authors contributions

GP, CJ, SK, and DK designed the research; GP, CJ, DR, MY, AB, DA, QZ, RB, SJ, LL, YS, and AT performed the research and data analysis; PPG and KKW provided materials; GP, CJ, SK, and DK wrote the manuscript; SK and DK were responsible for oversight and leadership; and all authors discussed results and revised the manuscript.

Acknowledgments

This publication was supported by the National Cancer Institute of the NIH under award numbers R01CA097098, R01CA166480, and R21CA216553.

Address correspondence to: Donald Kufe, Dana-Farber Cancer Institute, Department of Medical Oncology, 450 Brookline Avenue, D830, Boston, Massachusetts 02215, USA. Phone: 617-632-3141; Email: donald_kufe@dfci.harvard.edu.

YS's present address is: Osaka Police Hospital, Department of Gastrointestinal Surgery, Tennoji, Osaka, Japan.

1. Kufe DW. Mucins in cancer: function, prognosis and therapy. *Nat Rev Cancer*. 2009;9(12):874–885.
2. Kufe DW. MUC1-C oncoprotein as a target in breast cancer: activation of signaling pathways and therapeutic approaches. *Oncogene*. 2013;32(9):1073–1081.
3. Cheever MA, et al. The prioritization of cancer antigens: a national cancer institute pilot project for the acceleration of translational research. *Clin Cancer Res*. 2009;15(17):5323–5337.
4. de Bono JS, et al. Phase I trial of a murine antibody to MUC1 in patients with metastatic cancer: evidence for the activation of humoral and cellular antitumor immunity. *Ann Oncol*. 2004;15(12):1825–1833.
5. Moreno M, Bontkes HJ, Scheper RJ, Kenemans P, Verheijen RH, von Mensdorff-Pouilly S. High level of MUC1 in serum of ovarian and breast cancer patients inhibits huHMFG-1 dependent cell-mediated cytotoxicity (ADCC). *Cancer Lett*. 2007;257(1):47–55.
6. Pegram MD, et al. Phase I dose escalation pharmacokinetic assessment of intravenous humanized anti-MUC1 antibody AS1402 in patients with advanced breast cancer. *Breast Cancer Res*. 2009;11(5):R73.
7. Ibrahim NK, et al. Randomized phase II trial of letrozole plus anti-MUC1 antibody AS1402 in hormone receptor-positive locally advanced or metastatic breast cancer. *Clin Cancer Res*. 2011;17(21):6822–6830.
8. Rajabi H, Kufe D. MUC1-C oncoprotein integrates a program of EMT, epigenetic reprogramming and immune evasion in human carcinomas. *Biochim Biophys Acta*. 2017;1868(1):117–122.
9. Ramasamy S, Duraisamy S, Barbashov S, Kawano T, Kharbanda S, Kufe D. The MUC1 and galectin-3 oncoproteins function in a microRNA-dependent regulatory loop. *Mol Cell*. 2007;27(6):992–1004.
10. Macao B, Johansson DG, Hansson GC, Härd T. Autoproteolysis coupled to protein folding in the SEA domain of the membrane-bound MUC1 mucin. *Nat Struct Mol Biol*. 2006;13(1):71–76.
11. Raina D, et al. Characterization of the MUC1-C cytoplasmic domain as a cancer target. *PLoS One*. 2015;10(8):e0135156.
12. Rajabi H, Hiraki M, Kufe D. MUC1-C activates polycomb repressive complexes and downregulates tumor suppressor genes in human cancer cells. *Oncogene*. 2018;37(16):2079–2088.
13. Bouillez A, et al. Inhibition of MUC1-C suppresses MYC expression and attenuates malignant growth in KRAS mutant lung adenocarcinomas. *Cancer Res*. 2016;76(6):1538–1548.
14. Bouillez A, et al. MUC1-C integrates PD-L1 induction with repression of immune effectors in non-small-cell lung cancer. *Oncogene*. 2017;36(28):4037–4046.
15. Maeda T, et al. MUC1-C induces PD-L1 and immune evasion in triple-negative breast cancer. *Cancer Res*. 2018;78(1):205–215.
16. Khodarev NN, et al. MUC1-induced transcriptional programs associated with tumorigenesis predict outcome in breast and lung cancer. *Cancer Res*. 2009;69(7):2833–2837.
17. Pitroda SP, Khodarev NN, Beckett MA, Kufe DW, Weichselbaum RR. MUC1-induced alterations in a lipid metabolic gene network predict response of human breast cancers to tamoxifen treatment. *Proc Natl Acad Sci USA*. 2009;106(14):5837–5841.
18. MacDermed DM, et al. MUC1-associated proliferation signature predicts outcomes in lung adenocarcinoma patients. *BMC Med Genomics*. 2010;3:16.
19. Ligtenberg MJ, Kruijshaar L, Buijs F, van Meijer M, Litvinov SV, Hilkens J. Cell-associated episialin is a complex containing two proteins derived from a common precursor. *J Biol Chem*. 1992;267(9):6171–6177.
20. Parry S, Silverman HS, McDermott K, Willis A, Hollingsworth MA, Harris A. Identification of MUC1 proteolytic cleavage sites in vivo. *Biochem Biophys Res Commun*. 2001;283(3):715–720.
21. Panchamoorthy G, Rehan H, Kharbanda A, Ahmad R, Kufe D. A monoclonal antibody against the oncogenic mucin 1 cytoplasmic domain. *Hybridoma (Larchmt)*. 2011;30(6):531–535.
22. Leng Y, et al. Nuclear import of the MUC1-C oncoprotein is mediated by nucleoporin Nup62. *J Biol Chem*. 2007;282(27):19321–19330.
23. Kharbanda A, et al. Targeting the oncogenic MUC1-C protein inhibits mutant EGFR-mediated signaling and survival in non-small cell lung cancer cells. *Clin Cancer Res*. 2014;20(21):5423–5434.
24. Rajabi H, et al. DNA methylation by DNMT1 and DNMT3b methyltransferases is driven by the MUC1-C oncoprotein in human carcinoma cells. *Oncogene*. 2016;35(50):6439–6445.
25. Rajabi H, et al. MUC1-C activates EZH2 expression and function in human cancer cells. *Sci Rep*. 2017;7(1):7481.
26. Rowse GJ, Tempero RM, VanLith ML, Hollingsworth MA, Gendler SJ. Tolerance and immunity to MUC1 in a human MUC1 transgenic murine model. *Cancer Res*. 1998;58(2):315–321.
27. Gong J, et al. Reversal of tolerance to human MUC1 antigen in MUC1 transgenic mice immunized with fusions of dendritic and carcinoma cells. *Proc Natl Acad Sci USA*. 1998;95(11):6279–6283.
28. Siroy A, et al. MUC1 is expressed at high frequency in early-stage basal-like triple-negative breast cancer. *Hum Pathol*. 2013;44(10):2159–2166.
29. Pichinuk E, et al. Antibody targeting of cell-bound MUC1 SEA domain kills tumor cells. *Cancer Res*. 2012;72(13):3324–3336.
30. Wu G, et al. A Mucin1 C-terminal subunit-directed monoclonal antibody targets overexpressed Mucin1 in breast cancer. *Theranostics*. 2018;8(1):78–91.
31. Bouillez A, et al. MUC1-C promotes the suppressive immune microenvironment in non-small cell lung cancer. *Oncoimmunology*. 2017;6(9):e1338998.
32. Liegel J, et al. Phase I/Ib trial of MUC1-C inhibitor GO-203-2C with decitabine in acute myeloid leukemia. NIH website. https://clinicaltrials.gov/ct2/show/NCT02204085. Accessed May 30, 2018.
33. Lizotte PH, et al. Multiparametric profiling of non-small-cell lung cancers reveals distinct immunophenotypes. *JCI Insight*. 2016;1(14):e89014.
34. Ando K, et al. Developing a phosphospecific IHC assay as a predictive biomarker for topoisomerase I Inhibitors. *J Histochem Cytochem*. 2018:22155418766503.
35. Doronina SO, et al. Development of potent monoclonal antibody auristatin conjugates for cancer therapy. *Nat Biotechnol*. 2003;21(7):778–784.
36. Doronina SO, et al. Enhanced activity of monomethylauristatin F through monoclonal antibody delivery: effects of linker technology on efficacy and toxicity. *Bioconjug Chem*. 2006;17(1):114–124.

37. Hamblett KJ, et al. Effects of drug loading on the antitumor activity of a monoclonal antibody drug conjugate. *Clin Cancer Res*. 2004;10(20):7063–7070.
38. Wang Y, et al. CDK7-dependent transcriptional addiction in triple-negative breast cancer. *Cell*. 2015;163(1):174–186.